ELSEVIER

Earth and Planetary Science Letters 173 (1999) 91–100

EPSL

www.elsevier.com/locate/epsl

Seismic tomography with P and S data reveals lateral variations in the rigidity of deep slabs

S. Widiyantoro [a,*], B.L.N. Kennett [b], R.D. van der Hilst [c]

[a] Department of Geophysics and Meteorology, Bandung Institute of Technology, Bandung, 40132, Indonesia
[b] Research School of Earth Sciences, The Australian National University, Canberra, ACT 0200, Australia
[c] Department of Earth, Atmospheric, and Planetary Sciences, Massachusetts Institute of Technology, Cambridge, MA 02139-4307, USA

Received 27 May 1999; revised version received 7 September 1999; accepted 8 September 1999

Abstract

Regional seismic tomography of the northwest Pacific island arcs using P- and S-wave arrival time data with similar path coverage reveals an oceanic lithospheric slab deflected in the mantle transition zone beneath the Izu Bonin region in good agreement with the results of earlier tomographic and other seismic studies in the region. The S-wave images, however, do not show clearly the deflection of the slab. This implies that the stagnant lithospheric slab in the transition zone is more likely a bulk-sound structure, which is strongly supported by our results from joint inversions for bulk-sound and shear wavespeeds. For the Izu Bonin region, where trench migration has been reported, the properties of the deflected slab lying on top of the 660 km discontinuity show strong bulk-sound and weak shear signatures in contrast to the descending slab itself. There is an indication in the shear images that a component of the former oceanic lithosphere is penetrating into the top of the lower mantle, suggesting that a slab split has occurred. © 1999 Elsevier Science B.V. All rights reserved.

Keywords: rigidity; slabs; tomography; P-waves; S-waves

1. Introduction

Deep subduction of the Pacific plate beneath Japan and other northwestern Pacific island arcs has been the focus of many pioneering studies of convective flow across the upper mantle transition zone. However, our knowledge of slab structure beneath this region is almost entirely based on the results of tomographic inversions of P-wave data [1–6]. Information from S-wave data would help characterize the inferred wavespeed variations but the studies done so far [4] have not produced good constraints on the slab structure, which is likely due to the high noise level of the International Seismological Centre (ISC) S-wave data and the fact that this phase is not used in their (or ISC's) source location procedures.

We have inverted both P- and S-wave time residuals for aspherical mantle structure beneath the region depicted in Fig. 1 using the global data set of Engdahl et al. [7]. The results of the inversion for shear structure largely confirm the inferences from the P-wave data, but there are also subtle differences. Consistent with results of previous studies [5,6,8] our P images suggest that the Mariana slab penetrates vertically into the lower mantle and that the Izu Bonin slab is deflected in the upper mantle transition zone. Intriguingly, while the S images cor-

* Corresponding author. Tel.: +62 22 216088; Fax: +62 22 214225; E-mail: sriwid@geoph.itb.ac.id

0012-821X/99/$ – see front matter © 1999 Elsevier Science B.V. All rights reserved.
PII: S0012-821X(99)00216-2

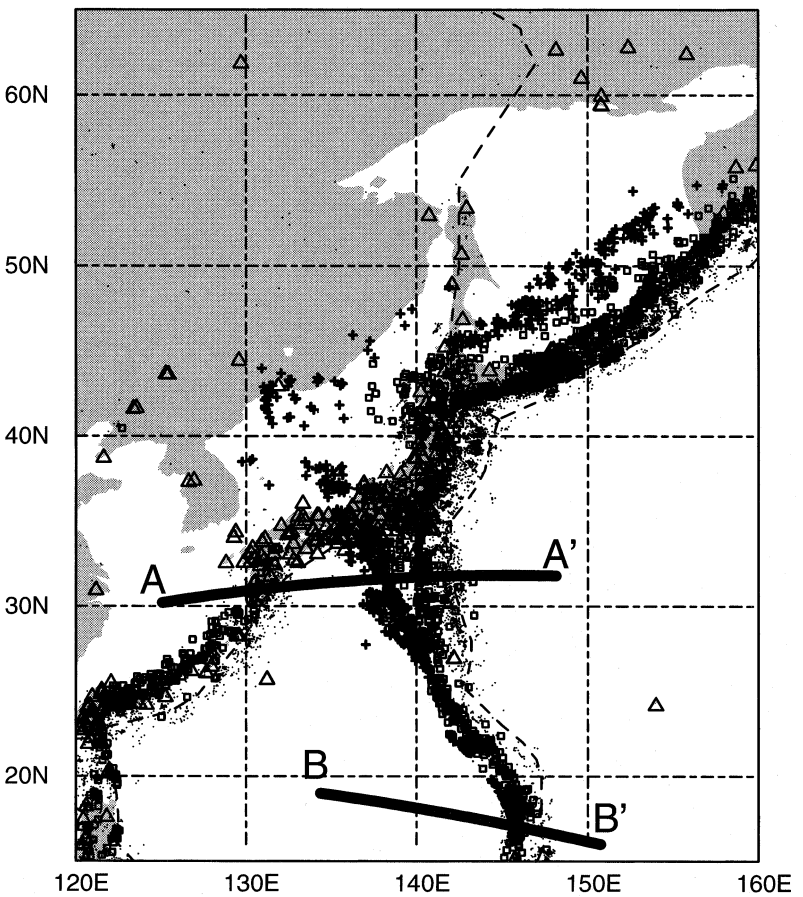

Fig. 1. Distribution of epicenters and seismographic stations within the study region. Open triangles depict stations that report both P and S data. Small dots, boxes and crosses depict epicenters of shallow ($0 < z \leq 70$ km), intermediate ($70 < z \leq 300$ km) and deep ($z > 300$ km) events, respectively, where z is the hypocenter depth. Solid lines indicate the positions of vertical cross-sections displayed in Figs. 3 and 5.

roborate the deep Mariana slab, first suggested by Creager and Jordan [9], they provide little evidence for the stagnant slab further north. Joint inversion of P- and S-wave data [10] also indicate that the deflected slab is primarily a bulk-sound feature and that its rigidity is small.

These observations are supported by results for the Tonga and Java subduction systems and suggest that stagnant slabs are less rigid than slab fragments that penetrate into the lower mantle [11]. Seismic tomography may thus sense variations in strength of the slab, which would open new opportunities for learning and provide an exciting new class of constraint for computer simulations of deep subduction.

2. P- and S-wave tomography

Using a nonlinear scheme and the radially stratified ak135 velocity model developed by Kennett et al. [12] and a total of about 13 million P, pP, pwP, PKP, and S phase arrival times reported by almost 6000 globally distributed seismographic stations, Engdahl et al. [7] carefully relocated almost 100,000 earthquakes that occurred between 1964 and 1995. In this study, we used an updated data set covering the period 1964 to 1998. This new data set has about 15% more data.

For our tomographic inversion of P and S travel time residuals we have used comparable ray cov-

erage for P and S to minimize the possibility that differences in compressional and shear wavespeed images are caused by the difference in the data sampling and effects of regularization. Most aspects of the tomographic imaging technique employed in this study have been described elsewhere [11,13,14]. Here we therefore provide only the most basic information.

From the global data sets we have selected P- and S-wave data with common event and station pairs to construct summary rays from event and station clusters based on $1^o \times 1^o$ regions and 50 km depth intervals for the event clusters. For events and stations inside the study area, we have used single rays for both P and S, and have selected almost every event and station pair with both P and S readings in order to optimize data coverage. For a ray to be included the travel time residual for P relative to the ak135 reference model has to lie in the range ± 5.0 s and the residual for S in the range ± 15.0 s. For each wave type we thus obtain 679,675 ray paths (397,395 summary rays and 282,280 individual rays) to constrain almost 120,000 unknowns as defined by the following model parameterization. We have used a cellular representation of mantle structure by discretizing the entire mantle using cells of $5^o \times 5^o$ (with 16 layers down to the bottom of the mantle), but in the study region we have employed a finer grid of $1^o \times 1^o$ (with 19 layers down to 1600 km) in order to allow the resolution of a relatively small-scale structure. Such a model parameterization minimizes contamination by structure outside the volume being investigated [6]. We end up with 116,360 unknowns (36,888 of which are associated with event relocation parameters upon inversion) to be solved using the iterative LSQR algorithm [15,16]. Upon inversion, which is linearized around the ak135 reference model [12], we achieved variance reductions of 47% for the P and 43% for the S travel time residuals. We remark that in the reprocessing of the ISC data undertaken by Engdahl et al. [7], which include source relocation and phase reidentification, a larger variance reduction was achieved for S data than for P data. The smaller variance reduction upon subsequent inversion probably reflects the larger component of measurement error in the S data compared with P.

3. Presentation of tomograms

The compressional and shear heterogeneity patterns in the transition zone (Fig. 2a,b) reveal high-wavespeed anomalies parallel to the present-day trench and shifted northwestward in agreement with the direction of Pacific plate motion. Interestingly, they also show some differences. In particular, the broadening beneath the Izu Bonin region in the map view of the P-wave image, which has previously been interpreted as a deflected slab, is not as pronounced in the S-wave image. To assess the significance of this difference we have performed a range of resolution tests in which we used the same P and S ray path coverage and inversion parameters as used in real data inversions. Gaussian random errors with a variance of 1.0 s^2 for P and 2.25 s^2 for S phases have been added to the calculated residual times. We also considered different sizes for the input anomalies to evaluate resolution at a range of length scales. Smaller structures are often resolved also, but for the purpose of this paper it suffices to note that the P and S data provide good constraints on structures larger than 2^o horizontal distance. As expected from the comparable data coverage the resolution in the P model is about the same as in the S model. In particular, Fig. 2c,d shows that the large-scale wavespeed variations in the transition zone beneath the Izu Bonin region are well constrained both by P and S data, suggesting that the inferred differences between the P and S images are real.

We further illustrate the differences between P and S structure in the transition zone by means of vertical sections across the Ryukyu and Izu Bonin subduction zones (Fig. 3a,b). We performed hypothesis tests to determine whether either the deep or the stagnant slabs can be artifacts owing to uneven sampling. To investigate whether the lower mantle slab in the S-image can result from the smearing of shallower structure we inverted travel time residuals that were calculated from an input model based on the original P result, but with velocity deviations set to zero for depths below 660 km (following [17]). From the results we conclude that although some low-amplitude smearing occurs, the upper mantle slab is not mapped into lower mantle anomalies along either P (Fig. 3c) or S rays (Fig. 3d). There are, however, subtle differences between the recov-

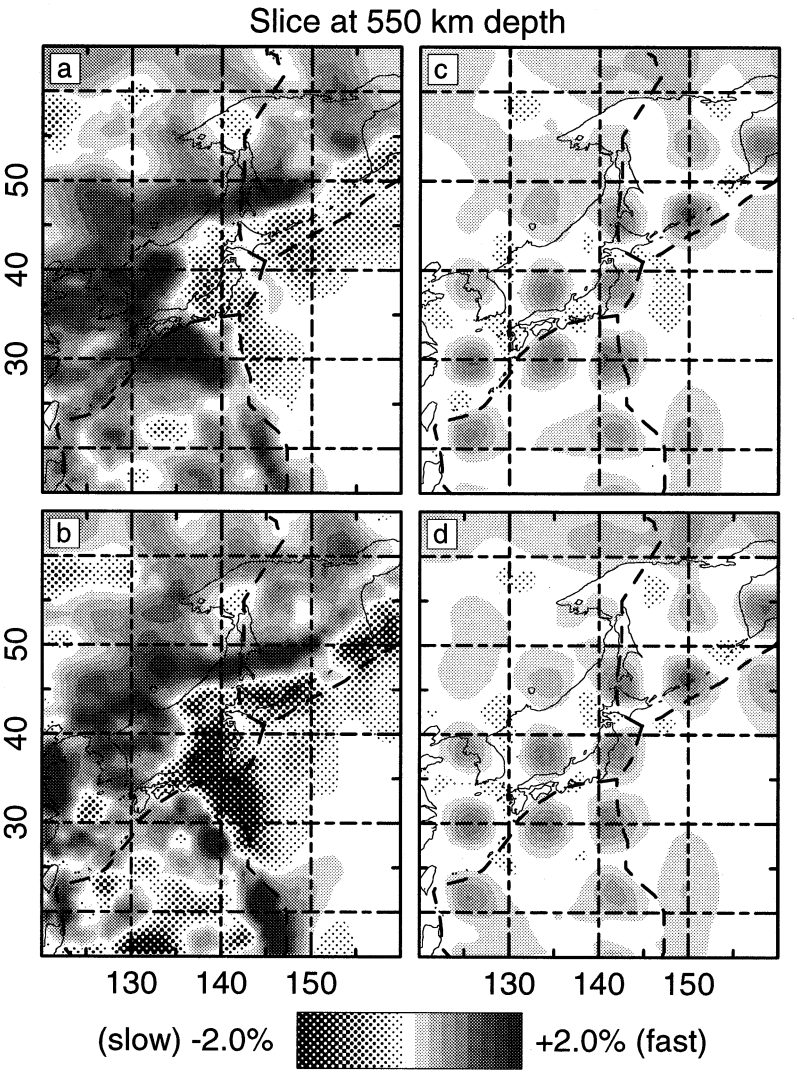

Fig. 2. Layer anomaly maps in the transition zone depicting results of the P and S data inversions. (a) P-wavespeed relative to ak135. (b) Same as (a), but inferred from S-wave information. (c) Recovery of a sensitivity test using a regular pattern ($4^o \times 4^o$) as the input model and the P ray paths as used in the real data inversion. Perturbations are set to +2.0% relative to ak135 inside the anomalies and zero outside. (d) Same as (c), except using S ray paths. Notice some loss of amplitude. The similarities between the recovery by P and S data derive from the use of comparable ray path coverage of the two different types of waves.

ered patterns using P- and S-wave data (Fig. 3c,d) arising from the differences in paths between P and S ray paths joining the same source and receiver. For the same focal depth and epicentral distance S rays will, in general, bottom deeper than P rays due to variations in the wavespeed ratio for the two types of waves as a function of depth. However, tests with the S model as input demonstrate that neither the use of P-ray paths nor the use of S-ray paths produce an artificial signal that resembles a deflected slab. These tests thus indicate that the differences between the P and S images presented here cannot be explained by differences in sampling by the P and S data.

The distinct differences in the patterns of P- and S-wave heterogeneity beneath the Izu Bonin region in Figs. 2 and 3 arise from distinct differences in

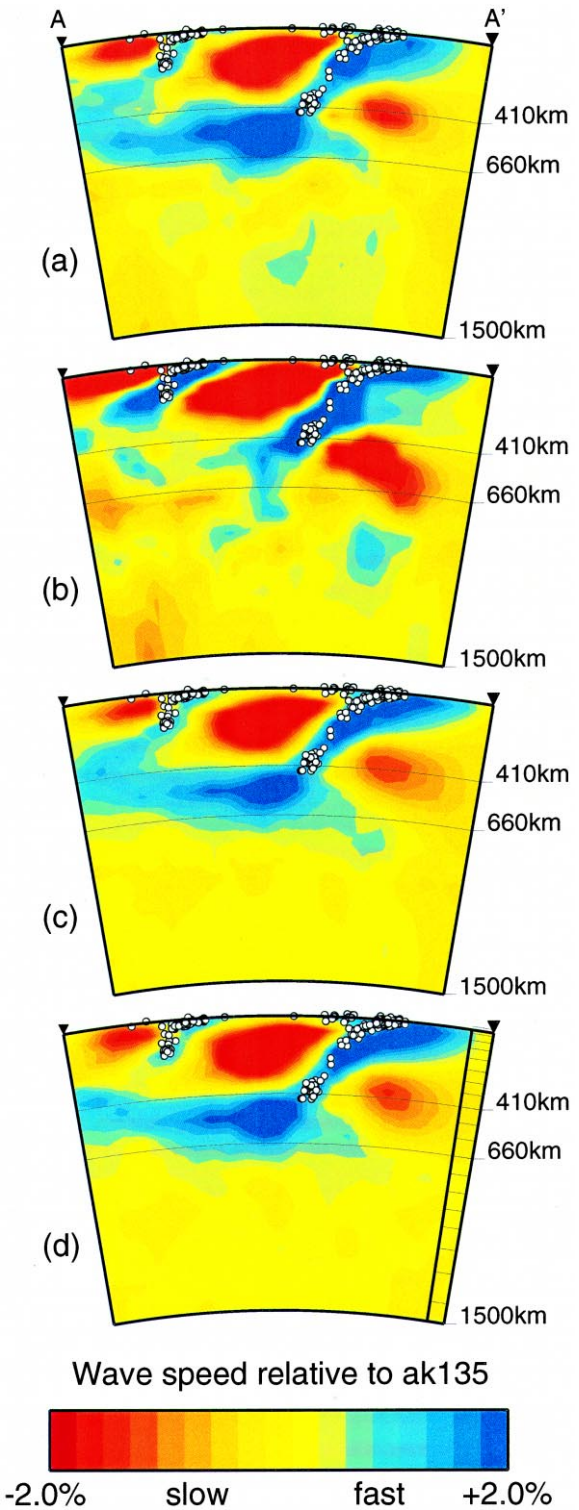

the characteristics of the P and S residuals patterns. In Fig. 4 we have extracted histograms of the P and S travel time residuals relative to the ak135 model for rays bottoming in the transition zone beneath Izu Bonin. The P-wave data clearly display relatively more 'large' negative residuals than for S, when we allow for the larger range of travel time residuals for S data. The behaviour of the histograms reflect directly the influence of structure in which the relative P wavespeed anomaly is somewhat larger than that in S. These travel time data come from events in the slab so that their character will have been imposed mostly by the anomalies associated with the presence of the flat-lying slab segment.

Although the images derived from P- and S-wave data show significant differences in the Izu Bonin region, this is not seen in the Marianas to the south. Vertical sections across the Mariana region from both P- and S-wave tomography are shown in Fig. 5; in each case we see a very clear image of slab penetration into the lower mantle. This suggests that the penetrating slab has higher rigidity than that deflected into the transition zone further north.

4. Discussion and conclusion

Results from joint tomographic inversion of P- and S-wave data for aspherical variations in bulk-sound and shear wavespeeds [10,11] strongly support the inference from the separate inversions that the deflected Izu Bonin slab has a strong influence on the bulk-sound speed (Fig. 6a) with only a weak presence in the shear model (Fig. 6b). These ob-

Fig. 3. Vertical cross-sections of tomographic images across Ryukyu and Izu Bonin. (a) P-wavespeed relative to ak135. (b) The same as (a), but inferred from S data. (c) Recovery by P-wave data of a hypothetical slab i.e. the model shown in (a) with perturbations set to zero for depths greater than 660 km (see text). (d) The same as (c), but recovered by using S-wave information. Notice that fast slab feature above the 660-km discontinuity is not mapped into lower mantle anomalies and smearing occurs with just small amplitudes. Open dots depict earthquake hypocenters of magnitude $\geq$5.5 on the Richter scale, projected from a distance of up to 50 km on both sides of the plane of section. The model parameterization in the radial direction is illustrated at the right side of (d).

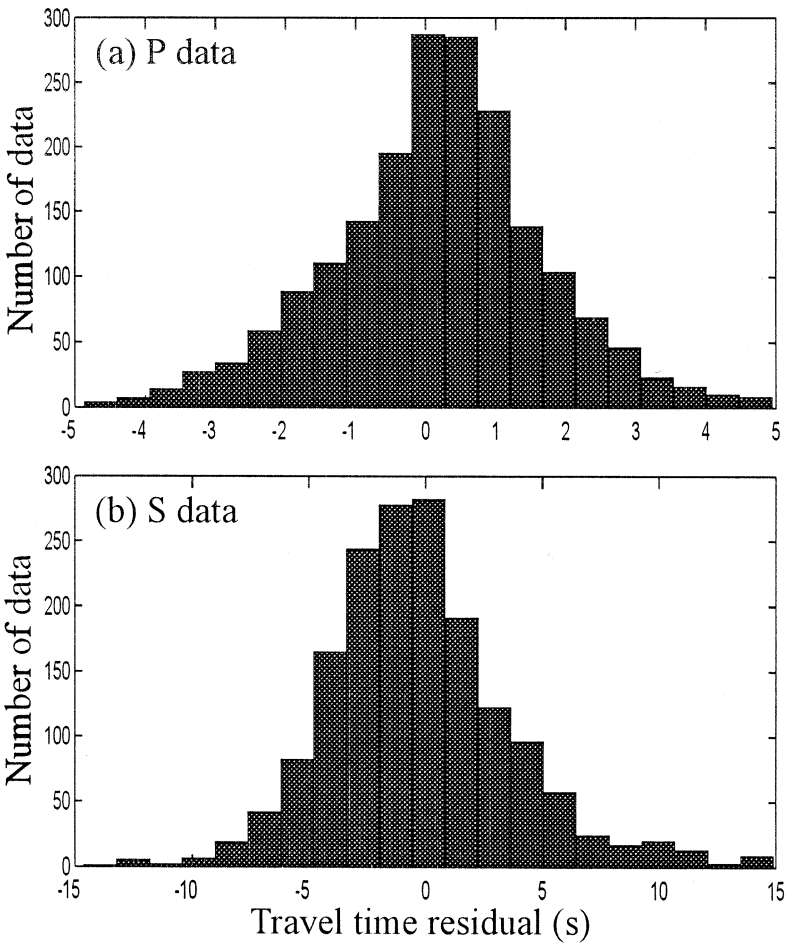

Fig. 4. Histograms of P- and S-wave travel time residuals (the difference between observed and calculated arrival times for the ak135 model) for rays bottoming in the transition zone beneath the Izu Bonin region, where the deflected slab lying on top of the 660 km discontinuity has been imaged.

servations suggest that variations in composition or rheology as well as thermal effects must contribute to the seismic signature of the stagnant slab below the Izu Bonin region, which is also associated with depression of the 660 km discontinuity [18].

Fig. 6 indicates that differences between the P- and S-wavespeed patterns are not restricted to the Izu Bonin region but also occur in other regions where subducted slabs have been reported to be (at least temporarily) stagnant in the transition zone, for instance beneath Sakhalin Island (north of Japan). Van der Hilst [17] reported that the descending slab beneath northern Tonga is deflected in the mantle transition region based on high-resolution regional P-wave tomography. Such a deflection is not depicted by S and SKS data even though the shear phases could resolve such a feature [19]. Comparing the bulk-sound and shear speed heterogeneity (Fig. 6) we infer that the deflected slab beneath Tonga is also a bulk-sound speed structure. In contrast, the deep slabs in the lower mantle beneath Java and the Marianas show up both in the P (and bulk-sound) and the S images.

In the joint tomographic inversions by Kennett et al. [10] from which the images in Fig. 6 have been extracted, data for paths where the absolute value of S travel time residuals exceeded 7.5 s were excluded. In contrast, in this study we have allowed

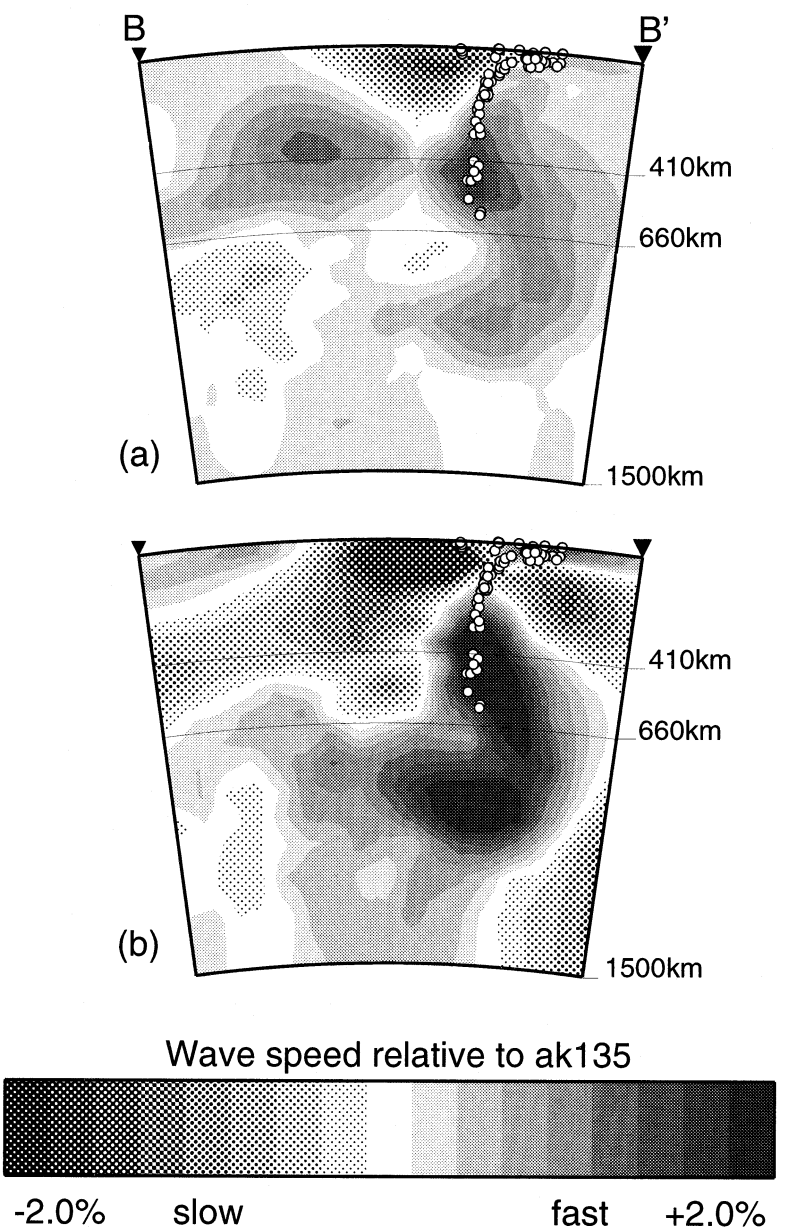

Fig. 5. Vertical cross-sections of tomographic images across the Mariana subduction zone. (a) P-wavespeed relative to ak135. (b) The same as (a), but inferred from S data. Notice the clear slab penetration into the lower mantle beneath the region both in the P- and S-wave images.

the absolute value of the S residuals to reach 15.0 s (Figs. 2, 3 and 5) in order to minimize possible bias arising from the strict constraint by including larger S wavespeed perturbations. However, the expansion of the S residual limit only adds about 5% additional data for this regional study and this has little influence on the nature of the images.

The images of seismic wavespeed have been constructed and displayed as deviations from the ak135 reference model [12], which has a simple upper man-

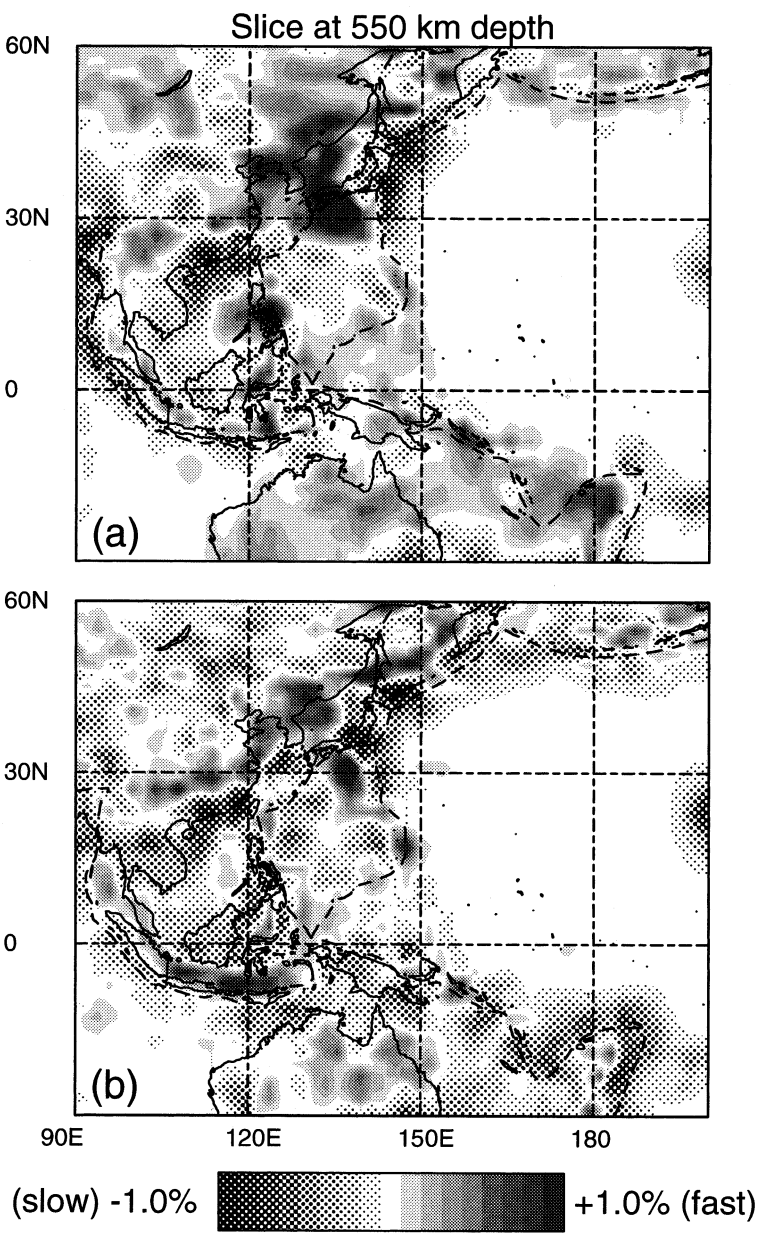

Fig. 6. Close-up of global bulk-sound and shear wavespeed models [10] for the layer anomaly map directly above the 660 km discontinuity in the western Pacific region. (a) Bulk-sound speed. (b) Shear wavespeed relative to ak135. Notice the broadening in bulk-sound map view of the fast slab beneath the northwest Pacific and Tonga, which does not exist in the shear model. Shear anomalies are pronounced beneath the Mariana and Java regions where subducted slabs directly penetrate into the lower mantle.

tle structure designed to model travel time behavior. Recent works on the amplitudes of PP and SS precursors [20,21] suggest that the ak135 model may overestimate the contrast at 660 km depth compared with the global average, whereas the S wavespeed jump may actually be larger. We therefore need to recognize the potential influence of the background model. If for example the images were displayed rel-

ative to the PREM model [22] there would be a little change close to 660 km depth in S, but the reference values of P-wave and bulk-sound speeds would be higher and so the positive anomalies associated with the slabs would be reduced. All tomographic images are dependent on the reference model but we are able to use the comparison of results for different regions in the same inversion as clear evidence for significant differences between the P and S behaviour between the Izu Bonin region and the Marianas.

Recent high-resolution global tomographic images [8,23,24] suggest that some slab fragments sink all the way down to the base of the mantle (or core–mantle boundary region). It has also been shown that some of the descending oceanic lithospheric slabs tend to lay flat on, across or below the 660 km discontinuity in some regions around the Pacific [5,6,25,26] and the Mediterranean [27]. Van der Hilst and Seno [28] suggested that slab deflection beneath some island arcs and slab penetration into the lower mantle below others can be related to the differences in the tectonic evolution of these subduction systems, in particular the amount and rate of trench retreat relative to the descending rate of the slab. This explanation has been corroborated by laboratory [29,30] and computer simulations [31–34]. The viscosity increase from upper to lower mantle and the dynamic effects of an endothermic phase change at 660 km depth both contribute to the dynamic feed-back between slab complexity and trench migration.

The inferred curvature of these slabs deflected in the transition zone implies low (flexural) rigidity. Riedle and Karato [35] argue that old (and cold) slabs, in particular, can develop weak zones owing to grain-size reduction associated with phase transformations, for instance near the tip of a metastable olivine wedge, which can facilitate and localize slab deflection. The lower rigidity of the deflected slab produced by this mechanism is consistent with our tomographic observations. However, the inference that some deep slabs are more rigid suggests that slab weakening is selective, implying that transformational grain-size reduction [35] is not the only mechanism.

Moreover, there is a suggestion of a weak shear anomaly associated with partial slab penetration into the lower mantle beneath the Izu Bonin region (Fig. 3b). This could be associated with a change in the style of subduction associated with relative plate motion (cf. the transition from ‘present’ to ‘future’ in fig. 7 of Van der Hilst and Seno [28]). Alternatively, the metastable wedge within the old slab may lead to splitting of the former oceanic lithosphere.

In conclusion, the combination of the P- and S-wave tomography on the regional scale with the global tomography results using a joint inversion for bulk-sound and shear wavespeed provides strong evidence for significant differences in the character of deflected slabs and those which penetrate into the lower mantle. The deflected slabs (Izu Bonin, Sakhalin, Tonga) show a strong bulk-sound perturbation but little signature in S implying low rigidity, whereas the slab fragments that show clear penetration into the lower mantle (Mariana, Java) have a strong shear signature.

Acknowledgements

We are very grateful to E.R. Engdahl for extensively refining the arrival-time information used in this study and Y. Fukao, S.P. Grand and T. Seno for carefully reading earlier versions of the manuscript and helpful comments. S.W. would like to thank JSPS for a Postdoctoral Fellowship (1998/1999) to conduct research at the Earthquake Research Institute, University of Tokyo where part of this work was done. ***[RV]***

References

[1] K. Hirahara, Three-dimensional seismic structure beneath southwest Japan: the subducting Philippine sea plate, Tectonophysics 79 (1981) 1–44.
[2] S. Kamiya, T. Miyatake, K. Hirahara, How deep can we see the high velocity anomalies beneath the Japan Islands?, Geophys. Res. Lett. 15 (1988) 828–831.
[3] W. Spakman, S. Stein, R.D. van der Hilst, R. Wortel, Resolution experiments for NW Pacific subduction zone tomography, Geophys. Res. Lett. 16 (1989) 1097–1101.
[4] H. Zhou, R.W. Clayton, P and S wave travel time inversions for subducting slabs under the island arcs of the northwest Pacific, J. Geophys. Res. 95 (1990) 6829–6851.
[5] R.D. van der Hilst, E.R. Engdahl, W. Spakman, G. Nolet, Tomographic imaging of subducted lithosphere below northwest Pacific island arcs, Nature 353 (1991) 37–43.

[6] Y. Fukao, M. Obayashi, H. Inoue, M. Nenbai, Subducting slabs stagnant in the mantle transition zone, J. Geophys. Res. 97 (1992) 4809–4822.
[7] E.R. Engdahl, R.D. van der Hilst, R. Buland, Global teleseismic earthquake relocation with improved travel times and procedures for depth determination, Bull. Seismol. Soc. Am. 88 (1998) 722–743.
[8] H. Bijwaard, W. Spakman, E.R. Engdahl, Closing the gap between regional and global travel time tomography, J. Geophys. Res. 103 (1998) 30055–30078.
[9] K. Creager, T.H. Jordan, Slab penetration into the lower mantle beneath the Mariana and other island arcs of the northwest Pacific, J. Geophys. Res. 91 (1986) 3573–3589.
[10] B.L.N. Kennett, S. Widiyantoro, R.D. van der Hilst, Joint seismic tomography for bulk-sound and shear wavespeed in the Earth's mantle, J. Geophys. Res. 103 (1998) 12469–12493.
[11] S. Widiyantoro, Studies of Seismic Tomography on Regional and Global Scale, Ph.D. Thesis, Australian National University, 1997, 256 pp.
[12] B.L.N. Kennett, E.R. Engdahl, R. Buland, Constraints on seismic velocities in the Earth from travel times, Geophys. J. Int. 122 (1995) 108–124.
[13] S. Widiyantoro, R.D. van der Hilst, Structure and evolution of lithospheric slab beneath the Sunda arc, Indonesia, Science 271 (1996) 1566–1570.
[14] S. Widiyantoro, R.D. van der Hilst, Mantle structure beneath Indonesia inferred from high-resolution tomographic imaging, Geophys. J. Int. 130 (1997) 167–182.
[15] C.C. Paige, M.A. Saunders, LSQR: an algorithm for sparse linear equations and sparse least squares, ACM Trans. Math. Soft. 8 (1982), pp. 43–71; pp. 195–209.
[16] G. Nolet, Seismic wave propagation and seismic tomography, in: G. Nolet (Ed.), Seismic Tomography, Reidel, Dordrecht, 1987, pp. 1–23.
[17] R.D. van der Hilst, Complex morphology of subducted lithosphere in the mantle beneath the Tonga trench, Nature 374 (1995) 154–157.
[18] P.M. Shearer, T.G. Masters, Global mapping of topography on the 660 km discontinuity, Nature 355 (1992) 791–796.
[19] S. Widiyantoro, B.L.N. Kennett, R.D. van der Hilst, Extending shear-wave tomography for the lower mantle using S and SKS arrival-time data, Earth Planets Space 50 (1998) 999–1012.
[20] C.H. Estabrook, R. Kind, The nature of the 660-km upper-mantle seismic discontinuity from precursors to the PP phase, Science 274 (1996) 1179–1182.
[21] P. Shearer, M.P. Flanagan, Resolving the average velocity and density jumps across upper-mantle discontinuities by modelling the range dependence of SS and PP precursors amplitudes, Eos 79 (45) (1998) F641.
[22] A.M. Dziewonski, D.L. Anderson, Preliminary reference Earth model, Phys. Earth Planet. Inter. 25 (1981) 297–356.
[23] S.P. Grand, R.D. van der Hilst, S. Widiyantoro, Global seismic tomography: a snapshot of convection in the Earth, Geol. Soc. Am. Today 7 (4) (1997) 1–7.
[24] R.D. van der Hilst, S. Widiyantoro, E.R. Engdahl, Evidence for deep mantle circulation from global tomography, Nature 386 (1997) 578–584.
[25] R.D. van der Hilst, S. Widiyantoro, K.C. Creager, T.J. McSweeney, Deep subduction and aspherical variations in P-wavespeed at the base of Earth's mantle, Geodynamics, AGU 28 (1998) 5–20.
[26] Y. Fukao, S. Widiyantoro, M. Obayashi, Stagnant slabs in the Bullen transition region, Eos 79 (45) (1998) F586.
[27] W. Spakman, S. van der Lee, R.D. van der Hilst, Travel-time tomography of the European–Mediterranean mantle down to 1400 km, Phys. Earth Planet. Inter. 79 (1993) 3–74.
[28] R.D. van der Hilst, T. Seno, Effects of relative plate motion on the deep structure and penetration depth of slabs below the Izu Bonin and Mariana island arcs, Earth Planet. Sci. Lett. 120 (1993) 395–407.
[29] C. Kincaid, P. Olson, An experimental study of subduction and slab migration, J. Geophys. Res. 92 (1987) 13832–13840.
[30] R.W. Griffiths, R.I. Hackney, R.D. van der Hilst, A laboratory investigation of effects of trench migration on the descent of subducted slabs, Earth Planet. Sci. Lett. 133 (1995) 1–17.
[31] M. Gurnis, B.H. Hager, Controls of the structure of subducted slabs, Nature 335 (1988) 317–321.
[32] G.F. Davies, Penetration of plates and plumes through the mantle transition zone, Earth Planet. Sci. Lett. 133 (1995) 507–516.
[33] S. Zhong, M. Gurnis, Mantle convection with plates and mobile, faulted plate margins, Science 267 (1995) 838–842.
[34] U.R. Christensen, The influence of trench migration on slab penetration into the lower mantle, Earth Planet. Sci. Lett. 140 (1996) 27–39.
[35] M.R. Riedel, S. Karato, Grain-size evolution in subducted oceanic lithosphere associated with the olivine–spinel transformation and its effects on rheology, Earth Planet. Sci. Lett. 148 (1997) 27–43.